

# Ultrafast optical Faraday effect in transparent solids

Michael S. Wismer,<sup>1,\*</sup> Mark I. Stockman,<sup>2,†</sup> and Vladislav S. Yakovlev<sup>1,3,‡</sup>

<sup>1</sup>Max-Planck-Institut für Quantenoptik, Hans-Kopfermann-Str. 1, 85748 Garching, Germany

<sup>2</sup>Center for Nano-Optics (CeNO) and Department of Physics and Astronomy,  
Georgia State University, Atlanta, Georgia 30340, USA

<sup>3</sup>Ludwig-Maximilians-Universität, Am Coulombwall 1, 85748 Garching, Germany

(Dated: September 1, 2022)

We demonstrate that a circularly polarized ultrashort laser pulse can induce a significant transient chirality in an achiral transparent dielectric. For moderate laser intensities, this is a  $\chi^{(3)}$  effect that vanishes under the assumption of an instantaneous nonlinear polarization response. For near-infrared laser fields as strong as  $\gtrsim 1 \text{ V/\AA}$ , nonperturbative electron dynamics become important. We propose to study these effects in time-resolved experiments by probing the induced transient chirality with a weak ultraviolet probe pulse that is shorter than an infrared pump pulse. Even in the nonperturbative regime, we observe the conservation of the spin angular momentum of photons in the spectral range well below the band edge, as well as a violation of this conservation law near the band edge.

## I. INTRODUCTION

In an optically inactive (achiral) isotropic medium, a weak linearly polarized light pulse preserves its polarization state as it propagates. However, even in such media, nonlinear interaction with a strong circularly polarized laser beam may rotate the polarization plane of the probe pulse, which is known as the *optical Faraday effect*<sup>1</sup>. Similarly to the Faraday effect and differently from optical activity in chiral media, the rotation angle  $\Delta\theta$  changes its sign if the propagation direction of the probe pulse is reversed. That is, the circularly polarized control field reduces the time-reversal symmetry. If the field also induces nonlinear absorption, it may induce circular dichroism, which changes the ellipticity of the propagated probe pulse.

This class of phenomena was first discovered in atomic vapors<sup>2-4</sup>. In those measurements, the frequencies of pump and probe pulses were tuned to atomic transitions, which enhanced the nonlinear interaction and, at the same time, rendered it nonparametric. Searching for new approaches to modulate light with light on femto- and attosecond time scales, we investigate the possibility and general properties of the optical Faraday effect in transparent solids, where both pulses are within the energy band gap. To the best of our knowledge, this regime has not yet been studied, even though nonlinear effects related to chirality were investigated on numerous occasions, including the optically probed inverse Faraday effect<sup>1,5,6</sup>, second-harmonic generation from achiral thin films<sup>7</sup>, nonlinear phenomena in chiral media<sup>8,9</sup>, self-induced polarization rotation<sup>10</sup>, ultrafast magneto-optics<sup>11</sup>, and high-harmonic generation from aligned molecules<sup>12</sup>. The purpose of this Letter is to close this knowledge gap. The nonlinear effects that we study are rather weak, which is probably the reason why they were often neglected in the past, but we show that they become significant for intense few-cycle laser pulses. Such pulses enable nondestructive measurements at peak intensities up to  $\sim 10^{14} \text{ W/cm}^2$ <sup>13</sup>, which opens up two op-

portunities: First, nonlinear light-matter interaction can be investigated using micrometer-thin samples<sup>14</sup>, where propagation effects play a minor role. Second, combined with the tools of attosecond metrology, intense few-cycle pulses make *nonperturbative* nonlinear phenomena accessible to time-resolved measurements. Examples of such processes include the Franz-Keldysh effect<sup>15-17</sup>, interband tunneling<sup>18</sup>, and high-harmonic generation<sup>19</sup>.

In the following, we consider pump-probe measurements where a circularly polarized few-cycle infrared (IR) pump pulse impinges at normal incidence on a uniaxial crystal (sapphire). We model light propagation along the optic axis, so that the linear optical properties of the crystal are effectively isotropic. The induced optical Faraday effect is probed by a linearly polarized ultraviolet (UV) pulse that is significantly shorter than the pump pulse, but not necessarily shorter than a single IR optical cycle. The probe pulse is sufficiently weak to neglect all nonlinear processes that involve more than one UV photon. For practical reasons, it may be beneficial to use a non-collinear geometry to spatially separate high-frequency components that the pump pulse may generate without any assistance from the probe pulse. Even in this case, the angle may be chosen small enough to neglect it while modeling propagation in a micrometer-thin sample.

## II. MODEL

We simulate electron dynamics in three spatial dimensions, working in the basis of stationary Bloch states in the velocity gauge. Within the dipole approximation, equations that describe electron dynamics at different crystal momenta  $\mathbf{k}$  are decoupled from each other,

$$i\hbar \frac{d}{dt} \hat{\rho}_{\mathbf{k}} = \left[ \hat{H}_{\mathbf{k}}^0 + \frac{e}{m_e} \mathbf{A}(t) \cdot \hat{\mathbf{p}}_{\mathbf{k}}, \hat{\rho}_{\mathbf{k}} \right]. \quad (1)$$

and the electric field  $\mathbf{F}(t)$  acting on electrons enters Eq. (1) via  $\mathbf{A}(t) = -\int_{-\infty}^t \mathbf{F}(t') dt'$ . We constructed

the unperturbed Hamiltonian  $H_{\mathbf{k}}^0$  from 36 valence bands (VB) and 160 conduction bands (CB) obtained in density-functional-theory calculations, which we performed for  $\text{Al}_2\text{O}_3$  using Wien2k<sup>20</sup>. The large number of bands is characteristic of velocity-gauge calculations<sup>21,22</sup>. The momentum matrix elements  $\hat{\mathbf{p}}_{\mathbf{k}}$  were likewise obtained from Wien2k. We used the modified Becke-Johnson exchange-correlation potential, which yields a band gap of  $E_g = 8.8$  eV, in agreement with experimental observations<sup>23</sup>.

We calculate the polarization response  $\mathbf{P}(t)$  by integrating the electric current density  $\mathbf{j}(t)$  with respect to time:  $\mathbf{P}(t) = \int_{-\infty}^t \mathbf{j}(t') dt'$ . The current density is evaluated as

$$\mathbf{j}^\alpha(t) = -\frac{2e}{m_e} \left( \frac{eN_0^\alpha}{V_{\text{cell}}} A^\alpha(t) + \int_{\text{BZ}} \frac{d^3k}{(2\pi)^3} \text{Tr} [\hat{\rho}_{\mathbf{k}}(t) \hat{\mathbf{p}}_{\mathbf{k}}^\alpha] \right), \quad (2)$$

where  $V_{\text{cell}}$  is the unit-cell volume, and

$$N_0^\alpha = \frac{2}{m_e} \sum_{i \in \text{CB}, j \in \text{VB}} \frac{|p_{ij}^\alpha|^2}{E_i - E_j} \quad (3)$$

is the effective number of electrons per unit cell for a given Cartesian component  $\alpha \in \{x, y, z\}$ <sup>24</sup>. This expression satisfies a requirement that  $\mathbf{P}(t)$  remains finite in the limit of the optical frequency tending to zero, while the amplitude of  $\mathbf{A}(t)$  is fixed. Using the effective number of electrons ensures that the Thomas-Reiche-Kuhn sum rule is satisfied for the approximations used. In particular, it reduces the number of bands required for obtaining numerically converged results.

We define the electric fields of the pulses via

$$\mathbf{F}^{\text{P}}(t) = \text{Re} [f^{\text{P}}(t) e^{-i\omega_{\text{P}} t} \mathbf{u}_{\text{P}}] = -d\mathbf{A}^{\text{P}}/dt, \quad (4)$$

$$\mathbf{A}^{\text{P}}(t) = F_{\text{P}} \omega_{\text{P}}^{-1} e^{-2 \ln(2)t^2/T_{\text{P}}^2} \text{Re} [i e^{-i\omega_{\text{P}} t} \mathbf{u}_{\text{P}}]. \quad (5)$$

Here,  $\text{P} \in \{\text{IR}, \text{UV}\}$ ,  $F_{\text{P}}$  is the amplitude of the electric field,  $T_{\text{P}}$  is the full width at half maximum of the pulse intensity, and the central pulse frequency is related to its central wavelength via  $\omega_{\text{P}} = 2\pi c/\lambda_{\text{P}}$ ,  $c$  being the vacuum speed of light. For the circularly polarized IR pump pulse, we used  $\lambda_{\text{IR}} = 750$  nm,  $\mathbf{u}_{\text{IR}} = (1, i, 0)$ , and  $T_{\text{IR}} = 5$  fs. For the linearly polarized UV probe pulse, we used  $\lambda_{\text{UV}} = 250$  nm,  $\mathbf{u}_{\text{UV}} = (1, 0, 0)$ ,  $T_{\text{UV}} = 2.5$  fs, and kept the peak field strength fixed at  $F_{\text{UV}} = 1$  mV/Å. Modeling pump-probe measurements, we introduce the delay,  $\tau$ , via the argument of the probe field:  $\mathbf{F}^{\text{UV}}(t - \tau)$ . In the following, we use Fresnel's formula,  $F_{\text{P}}^{\text{vac}} = \frac{1}{2}[1 + n(\omega_{\text{P}})]F_{\text{P}}$ , as an approximate relation between the vacuum amplitudes of the incident pulses,  $F_{\text{P}}^{\text{vac}}$ , and those within the crystal.

To calculate how the polarization state of the probe pulse changes during propagation, we first solve the first-order propagation equation for a distance that is small enough to neglect the distortion of the pump pulse. From the Fourier transform of the propagated field,  $\mathbf{F}^{\text{UV}}(\omega, z)$ ,

we evaluate the polarization angle as

$$\theta(\omega, z) = \frac{1}{2} \arcsin \left( \frac{2 \text{Re} \left[ (F_x^{\text{UV}}(\omega, z))^* F_y^{\text{UV}}(\omega, z) \right]}{|F^{\text{UV}}(\omega, z)|^2} \right). \quad (6)$$

We also define the ellipticity as  $\epsilon = \tan \chi_{\text{L}}$ , where  $\chi_{\text{L}}$  is the helicity given by<sup>25</sup>

$$\chi_{\text{L}}(\omega, z) = \frac{1}{2} \arcsin \left( \frac{2 \text{Im} \left[ (F_x^{\text{UV}}(\omega, z))^* F_y^{\text{UV}}(\omega, z) \right]}{|F^{\text{UV}}(\omega, z)|^2} \right). \quad (7)$$

If the probe pulse is initially polarized along the  $x$  axis, the derivatives of  $\theta$  and  $\epsilon$  with respect to the propagation distance are given by

$$\left. \left( \frac{\partial \theta}{\partial z} + i \frac{\partial \epsilon}{\partial z} \right) \right|_{z=0} = \frac{2\pi i \omega (F_x^{\text{UV}}(\omega, 0))^* P_y(\omega, 0)}{cn(\omega) |F_x^{\text{UV}}(\omega, 0)|^2}, \quad (8)$$

where  $n(\omega)$  is the refractive index (see Appendix B for more details).

### III. RESULTS AND DISCUSSION

Presenting our results, we first show how the optical Faraday effect depends on the strength of the IR field. The red curve in Fig. 1 illustrates the  $\partial\theta/\partial z \propto F_{\text{IR}}^2$  scaling in the weak-field limit, a range of laser fields where deviations from this scaling law become visible (above 0.1 V/Å), and typical values of the polarization rotation per unit propagation length. There results were obtained for pump and probe pulses arriving simultaneously ( $\tau = 0$ ). For a peak IR intensity of  $10^{13}$  W/cm<sup>2</sup>, the induced optical Faraday rotation at the central UV frequency is 0.03 radians (1.7°) per micrometer. Note that reaching this rotation strength in the conventional Faraday effect would require a magnetic field as strong as 700 Tesla, which exceeds the strongest nondestructive magnetic field currently available in laboratories. The blue curve in this figure illustrates that, in addition to this rotation, the UV pulse also experiences IR-pulse-induced circular dichroism. In the weak-field limit, the induced ellipticity per unit propagation length scales as  $\partial\epsilon/\partial z \propto F_{\text{IR}}^3$ , indicating that at least three IR photons must be absorbed in addition to a UV photon to overcome the band gap. At  $F_{\text{IR}} = 0.25$  V/Å, the induced zero-delay ellipticity changes its sign, which looks like a narrow downward spike on the logarithmic scale. Altogether,  $\partial\epsilon/\partial z \propto F_{\text{IR}}^3$  changes its sign four times in Fig. 1.

To clarify the origin of the induced chirality, we first review the relevant wave mixing processes within the standard framework of nonlinear optics, where the nonlinear polarization response in the vicinity of a frequency  $\omega = \omega_1 + \omega_2 + \omega_3$  is described by the third-order susceptibility tensor  $\chi_{ijkl}^{(3)}(\omega; \omega_1, \omega_2, \omega_3)$ . As long as the polarization response is linear with respect to the probe field,

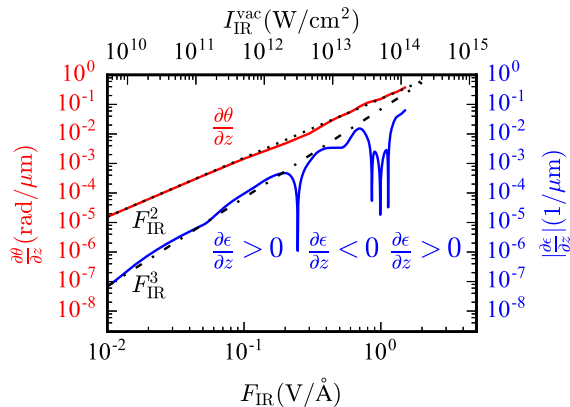


FIG. 1. The induced polarization rotation and circular dichroism at the central UV frequency for the zero delay between the pulses. The upper horizontal axis is labeled with peak intensities of the incident IR pulse in vacuum. For the lower horizontal axis, we used the peak IR field in the crystal at  $z = 0$ .

the optical Faraday effect is best understood by decomposing the linearly polarized UV pulse into its circularly polarized components:  $\mathbf{f}^{\text{UV}}(t) = \mathbf{e}_+ f_+^{\text{UV}}(t) + \mathbf{e}_- f_-^{\text{UV}}(t)$  with  $\mathbf{e}_\pm = (\hat{\mathbf{x}} \pm i\hat{\mathbf{y}})/\sqrt{2}$ . In the case  $\mathbf{f}^{\text{UV}}(t) \parallel \hat{\mathbf{x}}$ , we have  $f_+^{\text{UV}}(t) = f_-^{\text{UV}}(t) = \hat{\mathbf{x}} \cdot \mathbf{f}^{\text{UV}}(t)/\sqrt{2}$ . The pump pulse rotates the polarization plane of the probe pulse if it has different effects on its left- and right-rotating components. If there is a process that induces different absorption for the two components, circular dichroism is observed. Wave mixing processes that involve one UV photon and two IR photons also produce light at frequencies  $\omega_{\text{UV}} \pm 2\omega_{\text{IR}}$ . In a homogeneous isotropic medium, the spin angular momentum of a photon,  $\mathbf{S}$ , is conserved. From this principle, the following selection rules for third-order processes follow: (i) a circularly polarized IR field cannot generate the third-harmonic; (ii) both circularly polarized components of the UV pulse induce circularly polarized  $\mathbf{P}^{(3)}(\omega_{\text{UV}})$ , which rotates in the same direction as the UV field (in other words, absorbing and emitting an IR photon as a part of wave mixing does not change the spin angular momentum of the UV light); (iii) in the case of co-rotating IR and UV fields, emission at  $\omega_{\text{UV}} + 2\omega_{\text{IR}}$  is forbidden due to  $S \leq 1$ , while  $\mathbf{P}^{(3)}(\omega_{\text{UV}} - 2\omega_{\text{IR}})$  rotates in the direction opposite to that of the light fields; (iv) in the case of counter-rotating IR and UV fields, emission at  $\omega_{\text{UV}} - 2\omega_{\text{IR}}$  is forbidden, while  $\mathbf{P}^{(3)}(\omega_{\text{UV}} + 2\omega_{\text{IR}})$  rotates in the same direction as the IR field. We found that the same rules apply to the  $\bar{3}2/m$  crystal system of sapphire if the laser beam is aligned with its threefold rotation-inversion axis (see the Supplemental Material<sup>26</sup>), which is a nontrivial fact (for example, third-harmonic generation with circularly polarized light is allowed in cubic crystals, where the linear response is also isotropic).

If the wave mixing channels are spectrally separated,

effective susceptibilities,  $\chi_\pm^{\text{eff}} = \chi^{(1)} + \Delta\chi_\pm$ , describe the propagation of circularly polarized light at  $\omega = \omega_{\text{UV}}$ . For an IR field rotating counter-clockwise, we obtain<sup>26</sup>

$$\Delta\chi_\pm = 12F_{\text{IR}}^2 [\chi_{1111}^{(3)}(\omega_{\text{UV}}; -\omega_{\text{IR}}, \omega_{\text{IR}}, \omega_{\text{UV}}) - \chi_{2211}^{(3)}(\omega_{\text{UV}}; \mp\omega_{\text{IR}}, \pm\omega_{\text{IR}}, \omega_{\text{UV}})]. \quad (9)$$

Changing the helicity of the IR field replaces  $\Delta\chi_\pm$  with  $\Delta\chi_\mp$ . Optical Faraday effect emerges if  $\Delta\chi_- \neq \Delta\chi_+$ , which requires  $\chi_{2211}^{(3)}(\omega_{\text{UV}}; \omega_{\text{IR}}, -\omega_{\text{IR}}, \omega_{\text{UV}}) \neq \chi_{2211}^{(3)}(\omega_{\text{UV}}; -\omega_{\text{IR}}, \omega_{\text{IR}}, \omega_{\text{UV}})$ . The former susceptibility describes the process where an  $x$ -polarized IR photon is absorbed and a  $y$ -polarized photon is emitted (in addition to absorbing a UV photon), while the second one describes the opposite process. The two susceptibilities would be equal if the polarization response were instantaneous, in which case they would satisfy Kleinman's symmetry. Therefore, the optical Faraday effect is a consequence of the nonlinear polarization response being non-instantaneous.

We now turn our attention to the case of a field as strong as  $F_{\text{IR}} = 1 \text{ V/\AA}$ , where third-order susceptibilities no longer provide an accurate description of the optical Faraday effect (see Fig. 1). Fig. 2 shows that, even in this case, the three wave-mixing channels mentioned above are clearly visible. In Fig. 2(a), we use the logarithmic scale for polarization spectra, plotting the  $x$ - and  $y$ -components along the vertical and horizontal axes, respectively. The black curve represents the polarization  $\mathbf{P}^{\text{UV}}(\omega)$  induced by a sole UV pulse (note that we use  $\omega_{\text{UV}} = 3\omega_{\text{IR}}$ ). The area filled with the pale red color represents the polarization  $\mathbf{P}^{\text{IR}}(\omega)$  induced by the IR pulse alone. It illustrates that THG remains forbidden even for a field strong enough to excite some carriers into the conduction band and, by doing so, induce polarization response at frequencies above the band edge ( $\omega/\omega_{\text{IR}} \gtrsim 5.3$  in our simulations)<sup>27</sup>. Nevertheless,  $|\mathbf{P}^{\text{IR}}(\omega)|$  reaches significant values at frequencies close to  $3\omega_{\text{IR}}$ , which is why suppressing the IR-only response by using a noncollinear geometry may be required in experiments unless these contributions are sufficiently suppressed by phase matching. We model this suppression by subtracting the IR-only response. The areas filled with green and blue colors show  $|P_x(\omega) - P_x^{\text{IR}}(\omega)|$  and  $|P_y(\omega) - P_y^{\text{IR}}(\omega)|$ , respectively.

We obtain further insight by decomposing both the UV pulse and the polarization response into components with positive and negative helicities:  $\mathbf{P}(\omega) - \mathbf{P}^{\text{IR}}(\omega) = \mathbf{e}_+ P_+(\omega) + \mathbf{e}_- P_-(\omega)$ . The result is shown in Fig. 2(b). The subscript in  $P_\pm^{(\pm)}$  refers to the helicity of the polarization response, while the superscript denotes the helicity of the probe pulse. For example,  $P_+^{(-)}$ , which is the red line, shows the counter-clockwise rotating component of the polarization response that would be generated by a clockwise rotating UV field. Well below the band edge, the selection rules derived for the third-order perturbative response remain valid in the strong-field regime. In particular,  $|P_+^{(-)}(\omega)|^2$  is negligibly small at  $\omega_{\text{UV}}$  and

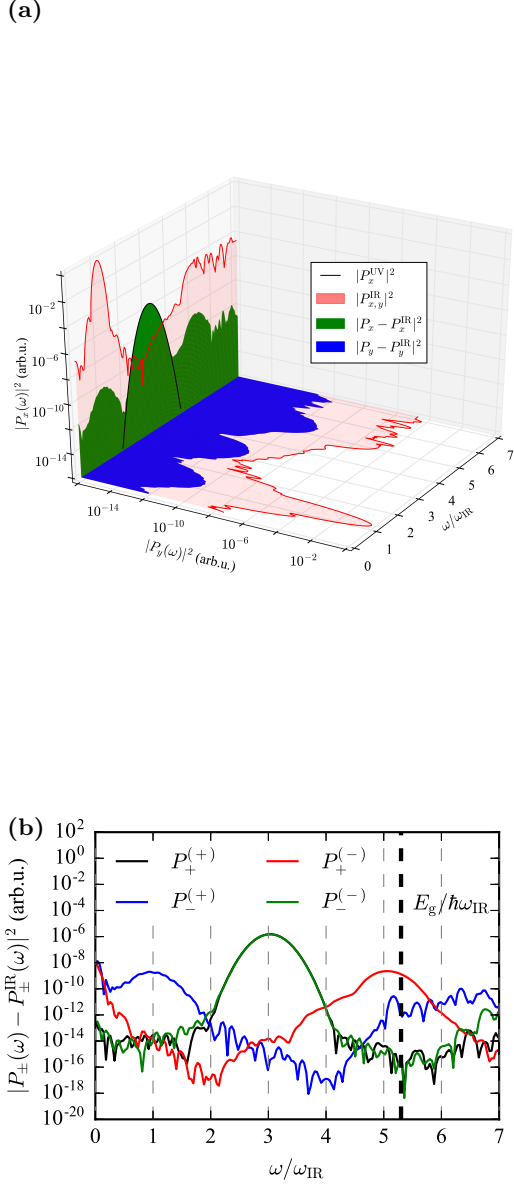


FIG. 2. The spectral analysis of the polarization response for  $F_{\text{IR}} = 1 \text{ V/\AA}$  and the zero pump-probe delay. The vertical black dashed line shows the position of the band edge. (a) The  $x$  and  $y$  components of the IR-only response  $\mathbf{P}^{\text{IR}}$  (pale red), the UV-only response  $\mathbf{P}^{\text{UV}}$  (black curve), and the polarization induced by both pulses after subtracting the IR-only response:  $\mathbf{P} - \mathbf{P}^{\text{IR}}$  (the green and blue areas). All the curves are plotted on the same scale. (b) The decomposition of  $\mathbf{P} - \mathbf{P}^{\text{IR}}$  into the left- and right-rotating components induced by the left- and right-rotating components of the UV pulse (see the text for further details).

$\omega_{\text{UV}} - 2\omega_{\text{IR}}$ , contributing mainly at  $\omega_{\text{UV}} + 2\omega_{\text{IR}} = 5\omega_{\text{IR}}$ . Near the band edge, the conservation of the photon spin is partially violated by  $P_-^{(+)}$  (blue line). For co-rotating field (the green and black curves), the polarization response is very weak at the band edge in spite of the coher-

ent excitations. A multiphoton process where total angular momentum of photons is not conserved requires that some angular momentum must be transferred to charge carriers. In this case, the medium itself is expected to acquire chiral properties.

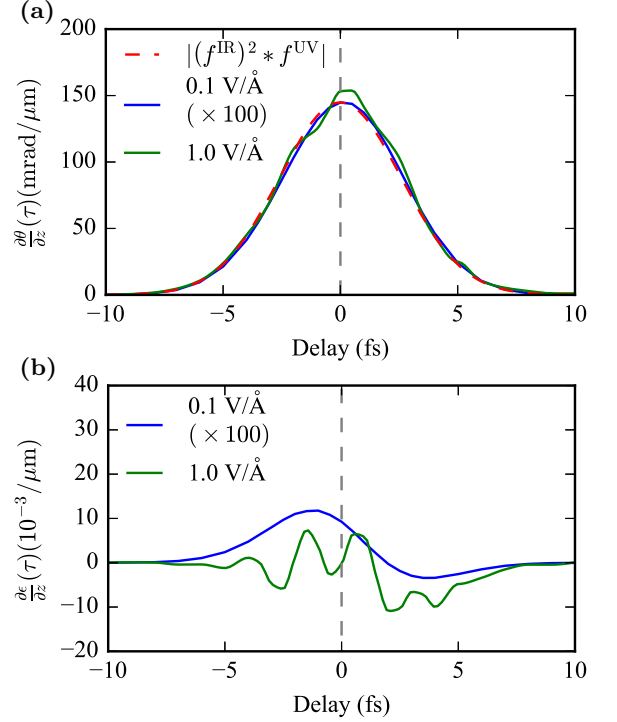


FIG. 3. The dependence of induced (a) polarization rotation and (b) ellipticity of the probe pulse on the pump-probe delay. In both panels, data for  $F_{\text{IR}} = 0.1 \text{ V/\AA}$  (blue curves) was multiplied by a factor of 100 to make it comparable to that for  $F_{\text{IR}} = 1 \text{ V/\AA}$  (green curves). In panel (a), the dashed red curve shows the convolution between the UV envelope and the square of the IR envelope.

Since the optical Faraday effect results from the nonlinear medium response being noninstantaneous, these effects lend themselves to pump-probe measurements. In Fig. 3(a), we show the delay dependence of the polarization rotation evaluated at the central UV frequency. Positive delays here mean that the probe pulse arrives after the pump pulse. At  $F_{\text{IR}} = 0.1 \text{ V/\AA}$ , the conventional perturbative nonlinear optics works well (see Fig. 1), so we expect  $\partial\theta/\partial z \propto F_{\text{IR}}^2$ . It is therefore not surprising that  $\partial\theta/\partial z$  as a function of the delay (blue curve) has precisely the same shape as the convolution  $|(f^{\text{IR}})^2 * f^{\text{UV}}|$  (red dashed curve). When we increase  $F_{\text{IR}}$  to  $1 \text{ V/\AA}$ , we observe a small but significant reshaping of  $\partial\theta/\partial z$ , revealing the onset of nonadiabatic processes that disappear by the end of the pulse. Our analysis of the results presented in Fig. 2, as well as the observation that reshaping is stronger at positive delays, suggest that these effects are probably related to the creation of real (nonvirtual) electronic excitations and angular momentum transfer from

photons to charge carriers. For  $1 \text{ V/\AA}$ , the residual excitation density is  $2.9 \times 10^{-5}$  electrons per unit cell. We also note that the dynamical Franz-Keldysh effect becomes an important excitation mechanism at such field strengths; nonadiabatic features of this effect have recently been predicted in numerical simulations<sup>17</sup>.

The nonadiabatic effects manifest themselves more vividly in the delay dependence of the induced ellipticity of the UV pulse. In Fig. 3(b), we show  $\partial\epsilon/\partial z$  evaluated with the aid of Eq. (8). When the IR field is weak ( $0.1 \text{ V/\AA}$ ), the induced ellipticity is mainly due to the time-dependent polarization rotation—the intensity of the 5-fs IR pulse changes significantly during the 2.5-fs UV pulse, and so does  $\partial\theta/\partial z$ . This contribution to the induced ellipticity is particularly large at delays where  $d|f^{\text{IR}}(\tau)|^2/d\tau$  is large. At the same time, even this relatively weak IR field induces some noticeable ellipticity at  $\tau = 0$ , where  $d|f^{\text{IR}}(\tau)|^2/d\tau = 0$ , and, therefore, the main mechanism is the induced circular dichroism. This contribution, which implies helicity-dependent absorption, has a qualitatively different delay dependence: it does not change sign at  $\tau = 0$ . The sum of the two functions, one of which is approximately odd and the other one is approximately even, results in the asymmetric shape of the blue curve. At  $F_{\text{IR}} = 1 \text{ V/\AA}$  (green curve), the induced ellipticity exhibits a complex, oscillatory dependence on the pump-probe delay, where the oscillation period is close to the optical period of the IR field (2.5 fs). Even in this regime, we do not observe any residual chirality—the induced ellipticity is only present when the pump and probe pulses overlap.

We now summarize our results and draw some conclusions. A strong adiabatic (i.e., with frequency within the band gap) circularly polarized optical field transiently changes the chiral properties of a dielectric. Specifically, we investigated the optical Faraday effect, where a circularly polarized IR pulse propagating along the optic axis of a sapphire crystal changes the polarization state of a co-propagating linearly polarized probe UV pulse. One property of this effect deserves a special emphasis: for any practical purposes, it is inertialess. Indeed, the time span of the pump-probe delay dependence in Fig. 3 is the same as the duration of the pump pulse, even if, within the pulse, the excitation of electrons to conduction bands changes the shape of  $\theta(\tau)$  and  $\epsilon(\tau)$ . This is in contrast to the optical Faraday effect in atoms, where selective excitation of magnetic sublevels by a circularly polarized pump pulse necessarily results in residual chirality. What makes the case of a solid qualitatively different is that averaging over crystal momenta in Eq. (2) leads to effective collisionless dephasing (Landau damping) that counteracts excitation-induced chirality. For basic research, the optical Faraday effect may be important as a spectroscopic tool for studying strong-field phenomena with an attosecond temporal resolution. Potential applications of this effect include ultrafast all-optical circular-polarization modulators, optical isolators, and optical circulators without a need for magnetic field.

## ACKNOWLEDGMENTS

M. S. W. was supported by the International Max Planck Research School of Advanced Photon Science (IMPRS-APS). V. S. Y. was supported by the DFG Cluster of Excellence: Munich-Centre for Advanced Photonics. His work at the GSU and CeNO on perturbative theory and preliminary numerical modeling was supported by a grant DE-SC0007043 from the Physical Behavior of Materials Program, Office of Basic Energy Sciences, U.S. Department of Energy. M. I. S. was supported by a MURI grant FA9550-15-1-0037 from the U.S. Airforce Office of Scientific Research. The authors gratefully acknowledge useful discussions with S. Kruchinin.

### Appendix A: Third-order polarization response

In this section, we provide some expressions for the third-order nonlinear polarization induced by a circularly polarized IR pulse and a weak linearly polarized UV pulse. We obtained these equations using the standard methods of nonlinear optics implemented in a Mathematica script. Doing so, we used the spatial symmetries of the  $\chi_{ijkl}^{(3)}$  tensor that correspond to a crystal with the sapphire symmetry ( $\bar{3}2/m$ ). We assume that both laser beams propagate along the crystal axis, which we chose to be the  $z$  axis of our coordinate system.

In the main text, we defined the complex pulse amplitude via  $\mathbf{F}^{\text{P}}(t) = \text{Re} [f^{\text{P}}(t)e^{-i\omega_{\text{P}}t}\mathbf{u}_{\text{P}}]$ , where  $\text{P} \in \{\text{IR}, \text{UV}\}$ . Here, to be consistent with the notation most frequently used in nonlinear optics, we use a different definition:

$$\mathbf{F}^{\text{P}}(t) = f^{\text{P}}(t)e^{-i\omega_{\text{P}}t}\mathbf{u}_{\text{P}} + \text{c.c.} \quad (\text{A1})$$

We used an IR pulse with the positive helicity:  $\mathbf{u}_{\text{IR}} = (1, i, 0)$ . Even though we propose measurements with a linearly polarized probe pulse, it is instructive to decompose the pulse into its left- and right-rotating circularly polarized components:  $\mathbf{u}_{\text{IR}} = (1, \pm i, 0)$ . The sign on the right-hand side of this expression appears in the subscript of  $P_{\pm}^{(\pm)}(t)$  in the equations below, where we use the same convention as in the main text: the superscript refers to the helicity of the probe pulse, while the subscript refers to the helicity of the polarization response. At the central frequency of the UV pulse, we obtained the following expressions for the part of the third-order polarization response that mixes the IR and UV beams:

$$\begin{aligned} P_{+}^{(+)}(t; \omega_{\text{UV}}) &= 12\sqrt{2} [f^{\text{IR}}(t)]^2 f^{\text{UV}}(t) \\ &\times \left[ \chi_{1111}^{(3)}(\omega_{\text{UV}}; -\omega_{\text{IR}}, \omega_{\text{IR}}, \omega_{\text{UV}}) \right. \\ &\left. - \chi_{2211}^{(3)}(\omega_{\text{UV}}; -\omega_{\text{IR}}, \omega_{\text{IR}}, \omega_{\text{UV}}) \right] + \text{c.c.}, \quad (\text{A2}) \end{aligned}$$

$$P_-^{(-)}(t; \omega_{UV}) = 12\sqrt{2} [f^{\text{IR}}(t)]^2 f^{\text{UV}}(t) \\ \times \left[ \chi_{1111}^{(3)}(\omega_{UV}; -\omega_{\text{IR}}, \omega_{\text{IR}}, \omega_{UV}) \right. \\ \left. - \chi_{2211}^{(3)}(\omega_{UV}; \omega_{\text{IR}}, -\omega_{\text{IR}}, \omega_{UV}) \right] + \text{c.c.}, \quad (\text{A3})$$

$$P_+^{(-)}(t; \omega_{UV}) = P_-^{(+)}(t; \omega_{UV}) = 0. \quad (\text{A4})$$

Deriving these equations, we dropped terms that were nonlinear with respect to  $f^{\text{UV}}(t)$  because the UV pulse is assumed to be weak. Deviating from the notation used in the main text, we do not explicitly account for the delay. If the UV pulse is delayed by  $\tau$ , its envelope  $f^{\text{UV}}(t)$  must be replaced with  $f^{\text{UV}}(t - \tau)e^{i\omega_{UV}\tau}$ .

Absorbing a UV photon and two IR photons generates the following components of the nonlinear polarization:

$$P_+^{(-)}(t; \omega_{UV} + 2\omega_{\text{IR}}) = 12\sqrt{2} [f^{\text{IR}}(t)]^2 f^{\text{UV}}(t) \\ \times \chi_{2211}^{(3)}(\omega_{UV} + 2\omega_{\text{IR}}; \omega_{\text{IR}}, \omega_{\text{IR}}, \omega_{UV}) + \text{c.c.}, \quad (\text{A5})$$

$$P_+^{(+)}(t; \omega_{UV} + 2\omega_{\text{IR}}) = P_-^{(-)}(t; \omega_{UV} + 2\omega_{\text{IR}}) \\ = P_-^{(+)}(t; \omega_{UV} + 2\omega_{\text{IR}}) = 0. \quad (\text{A6})$$

Absorbing a UV photon and emitting two IR photons generates

$$P_-^{(+)}(t; \omega_{UV} - 2\omega_{\text{IR}}) = 12\sqrt{2} [f^{\text{IR}}(t)]^2 f^{\text{UV}}(t) \\ \times \chi_{2211}^{(3)}(\omega_{UV} - 2\omega_{\text{IR}}; -\omega_{\text{IR}}, -\omega_{\text{IR}}, \omega_{UV}) + \text{c.c.} \quad (\text{A7})$$

and

$$P_+^{(+)}(t; \omega_{UV} + 2\omega_{\text{IR}}) = P_-^{(-)}(t; \omega_{UV} + 2\omega_{\text{IR}}) \\ = P_+^{(-)}(t; \omega_{UV} + 2\omega_{\text{IR}}) = 0. \quad (\text{A8})$$

The  $x$ - and  $y$ -components of the polarization response can be evaluated as

$$P_x = (P_+ + P_-) / \sqrt{2}, \quad (\text{A9})$$

$$P_y = i(P_+ - P_-) / \sqrt{2}. \quad (\text{A10})$$

Using our Mathematica script, we explicitly verified that there is no third-harmonic generation by the circularly polarized IR pulse, even if we take the fifth-order terms into account.

## Appendix B: Propagation model

To evaluate the induced ellipticity and polarization rotation of the probe pulse, we need to model its propagation. For this purpose, we employed the first-order propagation equation in the slowly-evolving wave approximation<sup>28</sup>:

$$\frac{\partial \mathbf{F}}{\partial z} = ik(\omega) \mathbf{F}(z, \omega) + \frac{2\pi i \omega}{cn(\omega)} \mathbf{P}^{\text{NL}}(z, \omega). \quad (\text{B1})$$

Here, we use CGS units, neglect diffraction, define the Fourier transform according to

$$\mathcal{F}[f(t)] = \int_{-\infty}^{\infty} f(t) e^{i\omega t} dt, \quad (\text{B2})$$

and define the nonlinear polarization via

$$\mathbf{P}(z, \omega) = \hat{\chi}^{(1)}(\omega) \mathbf{F}(z, \omega) + \mathbf{P}^{\text{NL}}(z, \omega). \quad (\text{B3})$$

The wave vector for propagation along the crystal axis is given by

$$k(\omega) = \frac{\omega}{c} n(\omega), \quad (\text{B4})$$

where  $n(\omega) = \sqrt{1 + 4\pi\chi^{(1)}(\omega)}$  is the refractive index.

To obtain Eq. (8) in the main text, we consider a UV pulse that is initially polarized along the  $x$ -axis and notice that

$$\left. \left( \frac{\partial \theta}{\partial z} + i \frac{\partial \chi}{\partial z} \right) \right|_{z=0} = \frac{\partial}{\partial z} \left( \frac{(F_x^{\text{UV}})^* F_y^{\text{UV}}}{|\mathbf{F}^{\text{UV}}|^2} \right) \Big|_{z=0}. \quad (\text{B5})$$

With

$$F_y^{\text{UV}}(0, \omega) \equiv 0, \quad (\text{B6})$$

$$\frac{\partial F_x^{\text{UV}}}{\partial z} \Big|_{z=0} = ik(\omega) F_x^{\text{UV}}(0, \omega), \quad (\text{B7})$$

$$\frac{\partial F_y^{\text{UV}}}{\partial z} \Big|_{z=0} = \frac{2\pi i \omega}{cn(\omega)} P_y^{\text{NL}}(0, \omega), \quad (\text{B8})$$

and,

$$\frac{\partial |\mathbf{F}^{\text{UV}}|^2}{\partial z} \Big|_{z=0} = \\ 2\text{Re} \left[ (F_x^{\text{UV}})^* \frac{\partial F_x^{\text{UV}}}{\partial z} + (F_y^{\text{UV}})^* \frac{\partial F_y^{\text{UV}}}{\partial z} \right] \Big|_{z=0} = \\ - \frac{2\omega}{c} |F_x^{\text{UV}}(0, \omega)|^2 \text{Im}[n(\omega)], \quad (\text{B9})$$

we obtain, neglecting the linear absorption ( $\text{Im}[n(\omega)] = 0$ ),

$$\left. \left( \frac{\partial \theta}{\partial z} + i \frac{\partial \epsilon}{\partial z} \right) \right|_{z=0} = \frac{2\pi i \omega (F_x^{\text{UV}}(\omega, 0))^* P_y^{\text{NL}}(\omega, 0)}{cn(\omega) |F_x^{\text{UV}}(\omega, 0)|^2}. \quad (\text{B10})$$

If effective susceptibilities provide a good approximation for the nonlinear polarization at the UV frequency,  $P_{\pm}(z, \omega_{UV}) = \Delta\chi_{\pm} F_{\pm}^{\text{UV}}(z, \omega_{UV})$ , it is possible to obtain the following expression for the polarization rotation in an isotropic medium:

$$\frac{d\theta(z, \omega_{UV})}{dz} = \frac{2\pi\omega_{UV}}{c} \text{Re} \left[ \frac{\Delta\chi_- - \Delta\chi_+}{n(\omega_{UV})} \right]. \quad (\text{B11})$$

The right-hand side of this equation does not depend on the probe pulse. Using the explicit expressions for  $\Delta\chi_{\pm}$ , we see that optical Faraday effect exists if  $\chi_{2211}^{(3)}(\omega_{UV}; \omega_{\text{IR}}, -\omega_{\text{IR}}, \omega_{UV}) \neq \chi_{2211}^{(3)}(\omega_{UV}; -\omega_{\text{IR}}, \omega_{\text{IR}}, \omega_{UV})$ .

### Appendix C: Numerical simulations

We obtained the lattice constants for  $\text{Al}_2\text{O}_3$  from<sup>29</sup>. The density-functional-theory and dynamical calculations were performed on an unshifted Monkhorst-Pack grid with  $5 \times 5 \times 5$   $\mathbf{k}$ -points. For each  $\mathbf{k}$ -point, the initial mixed state can be written as a sum of independent valence-band wave functions:

$$\rho_{\mathbf{k}}(t) = \sum_i^{N_v} |\psi_{i,\mathbf{k}}(t)\rangle \langle \psi_{i,\mathbf{k}}(t)|. \quad (\text{C1})$$

While the density-matrix description allow us to write the key equations in a compact and general form, we obtain the same results by solving the time-dependent Schrödinger equation (TDSE), which requires less computation. We work in the interaction picture:

$$i\hbar \frac{d}{dt} |\tilde{\psi}_{i,\mathbf{k}}\rangle = \frac{e}{m_e} \mathbf{A}(t) \cdot \tilde{\mathbf{p}}_{\mathbf{k}} |\tilde{\psi}_{i,\mathbf{k}}\rangle, \quad (\text{C2})$$

where  $|\tilde{\psi}_{i,\mathbf{k}}\rangle = e^{i\hat{H}_0 t/\hbar} |\psi_{i,\mathbf{k}}\rangle$ ,  $\tilde{\mathbf{p}}_{\mathbf{k}} = e^{i\hat{H}_0 t/\hbar} \hat{\mathbf{p}}_{\mathbf{k}} e^{-i\hat{H}_0 t/\hbar}$ , and  $\hat{H}_0$  is the unperturbed Hamiltonian. We used the 4th-order Runge–Kutta scheme to solve Eq. (C2) for 36 valence bands and 160 conduction bands. Thus, we had  $36 \times 5 \times 5 \times 5 = 4500$  independent differential equations, each of which was solved in a basis of  $36 + 160 = 196$  stationary states. On a desktop computer (Intel Core 2 Duo E8400 3.00 GHz), solving the TDSE for a single  $\mathbf{k}$ -point and a particular initial (valence) band takes 12 seconds.

Our simulations used the following expression for the Hamiltonian:  $\hat{H}(t) = \hat{H}_{\mathbf{k}}^0 + \frac{e}{m_e} \mathbf{A}(t) \cdot \hat{\mathbf{p}}_{\mathbf{k}}$ . A trivial unitary transformation relates this Hamiltonian to another velocity-gauge Hamiltonian that is frequently encountered in the literature:  $\hat{H}_{\mathbf{k}}^0 + \frac{e}{m_e} \mathbf{A}(t) \cdot \hat{\mathbf{p}}_{\mathbf{k}} + e^2 A^2(t)$ . This transformation reads

$$|\psi\rangle = \exp \left[ \frac{ie^2}{2\hbar m_e} \int_{-\infty}^t A^2(t') dt' \right] |\psi'\rangle. \quad (\text{C3})$$

Therefore, dropping the  $e^2 A^2(t)$  term in the Hamiltonian does not introduce an additional approximation.

- 
- \* michael.wismer@mpq.mpg.de  
 † mstockman@gsu.edu  
 ‡ vladislav.yakovlev@mpq.mpg.de
- <sup>1</sup> P. Atkins and M. Miller, *Molecular Physics* **15**, 503 (1968).
  - <sup>2</sup> V. M. Arutunian, T. A. Papazian, A. V. Karmenian, S. P. Ishkhanian, and L. Kholts, *Z. Eksp. Teor. Fiz.* **68**, 44 (1975).
  - <sup>3</sup> P. F. Liao and G. C. Bjorklund, *Phys. Rev. A* **15**, 2009 (1977).
  - <sup>4</sup> T. Thirunamachandran, *Chem. Phys. Lett.* **49**, 536 (1977).
  - <sup>5</sup> Y. Svirko and N. Zheludev, *Polarization of Light in Non-linear Optics* (Wiley, 1998).
  - <sup>6</sup> D. Cho, J. M. Choi, J. M. Kim, and Q.-H. Park, *Phys. Rev. A* **72**, 023821 (2005).
  - <sup>7</sup> T. Verbiest, M. Kauranen, and A. Persoons, *Phys. Rev. Lett.* **82**, 3601 (1999).
  - <sup>8</sup> P. Fischer and F. Hache, *Chirality* **17**, 421 (2005).
  - <sup>9</sup> L. M. Hauptert and G. J. Simpson, *Ann. Rev. Phys. Chem.* **60**, 345 (2009).
  - <sup>10</sup> N. Minkovski, G. I. Petrov, S. M. Satiel, O. Albert, and J. Etchepare, *J. Opt. Soc. Am. B* **21**, 1659 (2004).
  - <sup>11</sup> B. Koopmans, M. van Kampen, J. T. Kohlhepp, and W. J. M. de Jonge, *Phys. Rev. Lett.* **85**, 844 (2000).
  - <sup>12</sup> O. Smirnova, S. Patchkovskii, Y. Mairesse, N. Dudovich, D. Villeneuve, P. Corkum, and M. Y. Ivanov, *Phys. Rev. Lett.* **102**, 063601 (2009).
  - <sup>13</sup> M. Schultze, E. M. Bothschafter, A. Sommer, S. Holzner, W. Schweinberger, M. Fiess, M. Hofstetter, R. Kienberger, V. Apalkov, V. S. Yakovlev, M. I. Stockman, and F. Krausz, *Nature* **493**, 75 (2013).
  - <sup>14</sup> A. Sommer, E. M. Bothschafter, S. A. Sato, C. Jakubeit, T. Latka, O. Razskazovskaya, H. Fattahi, M. Jobst, W. Schweinberger, V. Shirvanyan, V. S. Yakovlev, R. Kienberger, K. Yabana, N. Karpowicz, M. Schultze, and F. Krausz, *Nature* **534**, 86 (2016).
  - <sup>15</sup> W. Franz, *Z. Naturforschung A* **13**, 484 (1958).
  - <sup>16</sup> L. Keldysh, *J. Experimentl. Theor. Phys.* **34**, 5, 1138-1141 (1958); Translation: *Sov. Phys. JETP* **7**, 788 (1958).
  - <sup>17</sup> T. Otobe, Y. Shinohara, S. A. Sato, and K. Yabana, *Phys. Rev. B* **93**, 045124 (2016).
  - <sup>18</sup> M. Gertszov, M. Spanner, D. M. Rayner, and P. B. Corkum, *J. Phys. B* **43**, 131002 (2010).
  - <sup>19</sup> S. Ghimire, A. D. DiChiara, E. Sistrunk, G. Ndabashimiye, U. B. Szafruga, A. Mohammad, P. Agostini, L. F. DiMauro, and D. A. Reis, *Phys. Rev. A* **85**, 043836 (2012).
  - <sup>20</sup> K. Schwarz, P. Blaha, and G. Madsen, *Computer Physics Communications* **147**, 71 (2002).
  - <sup>21</sup> M. Wu, S. Ghimire, D. A. Reis, K. J. Schafer, and M. B. Gaarde, *Phys. Rev. A* **91**, 043839 (2015).
  - <sup>22</sup> V. S. Yakovlev, S. Y. Kruchinin, T. Paasch-Colberg, M. I. Stockman, and F. Krausz, in *Ultrafast Dynamics Driven by Intense Light Pulses* (Springer, 2016) pp. 295–315.
  - <sup>23</sup> J. Olivier and R. Poirier, *Surface Science* **105**, 347 (1981).
  - <sup>24</sup> C. Ambrosch-Draxl and J. O. Sofo, *Computer Physics Communications* **175**, 1 (2006).
  - <sup>25</sup> A. Ferré, C. Handschin, M. Dumergue, F. Burgy, A. Comby, D. Descamps, B. Fabre, G. A. Garcia, R. Géneaux, L. Merceron, E. Mével, L. Nahon, S. Petit, B. Pons, D. Staedter, S. Weber, T. Ruchon, V. Blanchet, and Y. Mairesse, *Nature Photonics* **9**, 93 (2015).
  - <sup>26</sup> See Supplemental Material at [URL will be inserted by publisher], which includes references<sup>28,29</sup>, for details of our numerical model and some expressions for the third-order nonlinear polarization.
  - <sup>27</sup> M. Korbman, S. Y. Kruchinin, and V. S. Yakovlev, *New J. Phys.* **15**, 013006 (2013).
  - <sup>28</sup> T. Brabec and F. Krausz, *Rev. Mod. Phys.* **72**, 545 (2000).
  - <sup>29</sup> X.-L. Wang, C. R. Hubbard, K. B. Alexander, P. F. Becher, J. A. Fernandez-Baca, and S. Spooner, *Journal of the American Ceramic Society* **77**, 1569 (1994).